PROCEEDINGS OF SPIE

Improving self super resolution in magnetic resonance images

Sachin Goyal, Can Zhao, Amod Jog, Jerry L. Prince, Aaron Carass

Improving Self Super Resolution in
Magnetic Resonance Images

Sachin Goyal[a], Can Zhao[b], Amod Jog[c], Jerry L. Prince[b, d], and Aaron Carass[b, d]

[a]Dept. of Electrical Engineering, Indian Institute of Technology, Bombay, Maharashtra, India
[b]Dept. of Electrical and Computer Engineering,
The Johns Hopkins University, Baltimore, MD 21218, USA
[c]Athinoula A. Martinos Center for Biomedical Imaging,
Massachusetts General Hospital, Charlestown, MA 02129, USA
[d]Dept. of Computer Science, The Johns Hopkins University, Baltimore, MD 21218, USA

ABSTRACT

Magnetic resonance (MR) images (MRI) are routinely acquired with high in-plane resolution and lower through-plane resolution. Improving the resolution of such data can be achieved through post-processing techniques knows as super-resolution (SR), with various frameworks in existence. Many of these approaches rely on external databases from which SR methods infer relationships between low and high resolution data. The concept of self super-resolution (SSR) has been previously reported, wherein there is no external training data with the method only relying on the acquired image. The approach involves extracting image patches from the acquired image constructing new images based on regression and combining the new images by Fourier Burst Accumulation. In this work, we present four improvements to our previously reported SSR approach. We demonstrate these improvements have a significant effect on improving image quality and the measured resolution.

Keywords: MRI, super-resolution, unsupervised methods

1. INTRODUCTION

Determining the acquisition resolution in magnetic resonance (MR) images (MRI) is an important step in the imaging system that can have dramatic consequences for the usability of a data set. The spatial resolution is chosen based on imaging time, desired signal to noise ratio, and other factors. However, spatial resolution is ultimately determined by the amount of k-space acquired in the Fourier domain. Seeking post-acquisition ways to improve the resolution of MR images has been an active area of research for three decades.[1–15] Super-resolution (SR), as this is known, is the process through which we estimate high frequency information that is not acquired during the imaging at lower resolutions.

MR images are typically upsampled to an isotropic resolution having been acquired with high in-plane and low-through plane resolution. This results in images with partial volume artifacts that lead to degraded image analysis in subsequent processing. There have been many approaches to SR in medical imaging, see the review papers.[16, 17] SR techniques in medical imaging include model based,[4] and regression[11] using random forests[12] and deep learning.[14, 15] Model based approaches suffer from the inherent ill-posed nature of the problem. Regression work can have issues matching the contrast between the training data and the data from the new subjects, though there has been work[18] that can adaptively update the training data to avoid contrast mismatches. Model based approaches, which are ill-posed, have begun to be replaced by regression based work, which itself has issues with the contrast between the training data and new subjects not matching. To avoid these issues, there has been exploration of self super-resolution (SSR)—where the test data itself is suitably transformed and used to train the regression models. For example, Huang et al.[19] downsample an input image and learn a regression between the downsampled image and the original input image. This regression is then applied to original input image to

Further author information: (Send correspondence to A. Carass)
A. Carass: E-mail: aaron_carass@jhu.edu

generate a higher resolution image. We note that Huang et al.[19] worked on natural images and attempts to learn regression in medical imaging[20] have depended on external training images.

Previously,[13] we described a method that only uses information from an available low resolution (LR) image to estimate its SR image in a truly SSR approach. Our SSR approach takes advantage of the fact that in an anisotropic acquisition, the in-plane resolution is higher than the through-plane resolution.

2. NEW WORK TO BE PRESENTED

In this work, we present four changes to our previously reported SSR method;[13] we refer to our new method as SSRv2 and our previously reported work as SSRv1.[13] SSRv1 comprised two steps: **1)** generating new additional images, each of which is LR along a certain direction, but is HR in the plane normal to it. Thus, each new image contributes information to a new region in the Fourier space. **2)** We combine these images in the Fourier space with Fourier Burst Accumulation (FBA).[21,22] We currently include a comparison between SSRv1 and SSRv2, noting that SSRv1 has been shown to be better than state-of-the-art SR methods.

3. METHODS

We briefly review Fourier Burst Accumulation (FBA)[21,22] and SSRv1, before introducing SSRv2.

Fourier Burst Accumulation Delbracio et al.[21,22] introduced the image deblurring method known as Fourier Burst Accumulation (FBA). Given a series of images of the same scene acquired in the burst mode of a digital camera, FBA recovers a single high resolution image with reduced noise. The assumption is that each burst image is blurred due to random motion blur introduced by hand tremors and the blurring directions are independent of each other. $\boldsymbol{x}$ is the unobserved true HR image, and $\boldsymbol{y}_i$ for $i = 1, \ldots, n$ the ith observed LR image—which is blurred in a random direction with kernel $\boldsymbol{h}_i$. So we have $\boldsymbol{y}_i = \boldsymbol{h}_i * \boldsymbol{x} + \boldsymbol{\sigma}_i$, where $\boldsymbol{\sigma}_i$ is the noise in the ith image. For the jth voxel of $\boldsymbol{x}$, the FBA estimate $\hat{\boldsymbol{x}}_p(j)$ is,

$$\hat{\boldsymbol{x}}_p(j) = \mathcal{F}^{-1}\left(\sum_{i=1}^{n} \boldsymbol{w}_i(\omega)\boldsymbol{Y}_i(\omega)\right)(j), \quad \text{where } \boldsymbol{w}_i(\omega) = \frac{|\boldsymbol{Y}_i(\omega)|^p}{\sum_{i=1}^{n}|\boldsymbol{Y}_i(\omega)|^p} \quad \text{and } \boldsymbol{Y}_i(\omega) = \mathcal{F}(\boldsymbol{y}_i). \tag{1}$$

Thus the Fourier transform of the high resolution image $\boldsymbol{x}$ is a weighted average of the Fourier transforms $\boldsymbol{Y}_i(\omega)$ of the input burst images. That is, given LR images blurred independently from the same HR image, an estimate of the underlying HR can be calculated using FBA.

SSRv1 For the SSR of MR images, the input is $\boldsymbol{y}$ and the desired SR output is $\hat{\boldsymbol{x}}$. We assume that $\boldsymbol{y}$ is LR in the through-plane (z-axis) direction and is HR in-plane. We denote the spatial resolution of $\boldsymbol{y}$ as $r_x \times r_y \times r_z$ mm^3, and assume that $r_z > r_x = r_y$. In Fourier space, the extent of the Fourier cube is $[-R_x, R_x]$, where $R_x = 1/2r_x$ mm^{-1} on the ω_x axis, $[-R_y, R_y]$, $R_y = 1/2r_y$ mm^{-1} on the ω_y axis, and $[-R_z, R_z]$ $R_z = 1/2r_z$ mm^{-1} on the ω_z axis. Clearly, $R_z < R_x = R_y$. To improve the resolution in the z direction, it is necessary to widen the Fourier limit on the ω_z axis by estimating the Fourier coefficients for frequencies that are greater than R_z. We use FBA for estimating the Fourier coefficients at these frequencies.

FBA requires multiple images as input and expects that some of the images have the Fourier coefficients in the desired region and uses those to fill in the missing Fourier information. It is impossible to perform FBA with just a single image $\boldsymbol{y}$ as there is no way to estimate the Fourier information outside of $[-R_z, R_z]$ on the ω_z axis. Thus, we need additional images that can provide higher frequency information on the ω_z axis. The first stage in our proposed SR algorithm is to create these additional images through synthesis given only $\boldsymbol{y}$.

To generate images from $\boldsymbol{y}$, which can be used by FBA and thus cover more high frequency portions of Fourier space, we use a regression framework with rotated and filtered versions of the available $\boldsymbol{y}$. We initially upsample $\boldsymbol{y}$ to an isotropic volume using cubic b-spline interpolation, and assume the following model, $\boldsymbol{y} = \boldsymbol{h} * \boldsymbol{x} + \boldsymbol{\sigma}$. Given rotation matrices M_i, $i \in \{1, \ldots, n\}$: 1) generate $M_i(\boldsymbol{y})$, $\boldsymbol{y}$ rotated by M_i; 2) apply the rotated kernel $M_i(\boldsymbol{h})$ to $\boldsymbol{y}$ to create $\boldsymbol{y}_i = M_i(\boldsymbol{h}) * \boldsymbol{y}$; 3) apply the kernel $\boldsymbol{h}$ to $M_i(\boldsymbol{y})$ to form $\widetilde{\boldsymbol{y}}_i = \boldsymbol{h} * M_i(\boldsymbol{y})$. Then for each M_i, we have two new images $\boldsymbol{y}_i$ and $\widetilde{\boldsymbol{y}}_i$. Ignoring noise, we can formulate $\boldsymbol{y}_i = M_i(\boldsymbol{h}) * \boldsymbol{y} = M_i(\boldsymbol{h}) * \boldsymbol{h} * \boldsymbol{x}$, and build a regression between $\boldsymbol{y}_i$ and $\boldsymbol{y}$ as training images by extracting patches from $\boldsymbol{y}_i$ and pairing them appropriately with patches
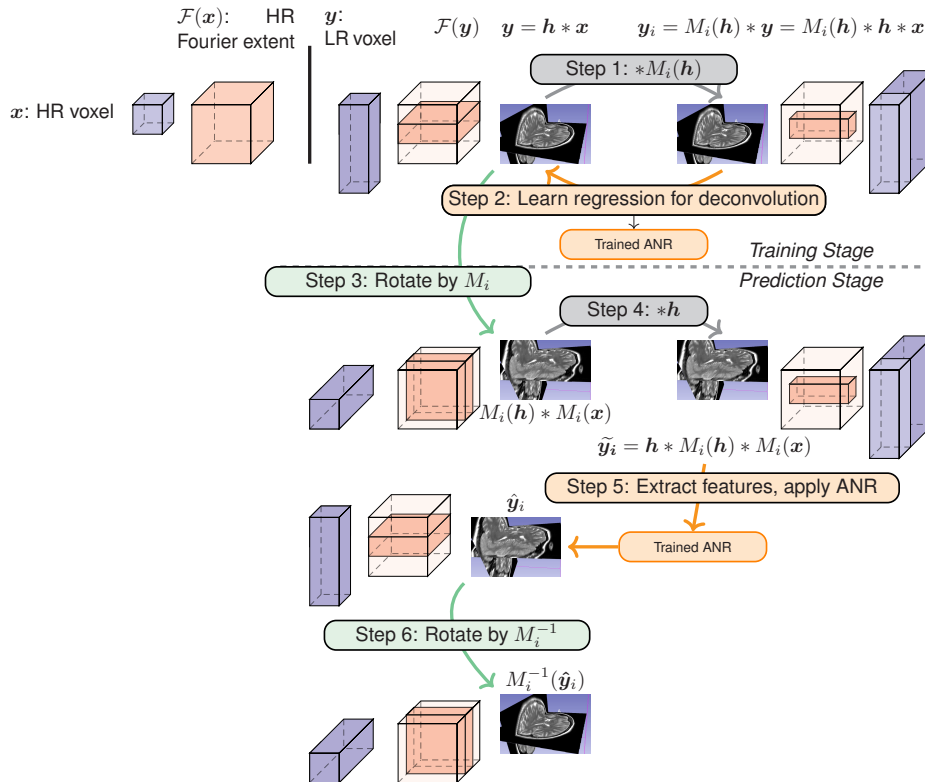
Figure 1. **Steps 1 and 2** show how to construct the training data from the input image, $\boldsymbol{y}$. **Steps 3 and 4** show how to generate the rotated images, $\widetilde{\boldsymbol{y_i}}$. **Step 5** shows how to synthesizing the images, $\hat{\boldsymbol{y_i}}$, that have different Fourier extents, and **Step 6** shows how to undo the rotations, so the images can be combined using the Fourier Burst Accumulation to generate the SR image $\hat{\boldsymbol{x}}_p = \text{FBA}(\boldsymbol{y}, M_1^{-1}(\hat{\boldsymbol{y}}_1), \ldots, M_n^{-1}(\hat{\boldsymbol{y}}_n), p)$.

in $\boldsymbol{y}$. Thus, we learn the transformation that deconvolves $\boldsymbol{y}_i$ to get $\boldsymbol{y}$, we then apply this learned deconvolution to $\widetilde{\boldsymbol{y}}_i$. Again ignoring noise, we note that $\widetilde{\boldsymbol{y}}_i = \boldsymbol{h} * M_i(\boldsymbol{y}) = \boldsymbol{h} * M_i(\boldsymbol{h} * \boldsymbol{x}) = \boldsymbol{h} * M_i(\boldsymbol{h}) * M_i(\boldsymbol{x})$. Thus deconvolving $\boldsymbol{y}_i$ to cancel the effects of $M_i(\boldsymbol{h})$ is analogous to deconvolving $\widetilde{\boldsymbol{y}}_i$ to cancel the effects of $\boldsymbol{h}$, as $\widetilde{\boldsymbol{y}}_i$ is also rotated. The regression is learned using Anchored Neighborhood Regression (ANR).[23] We provide a brief summary of ANR, complete details of which are in Timofte et al.[23] The training pair in ANR for each rotation M_i is $\boldsymbol{y}_i$ and $\boldsymbol{y}$, with the test image being $\widetilde{\boldsymbol{y_i}}$. ANR has been shown to be effective in 2D super-resolution of natural images with better results than some of the state-of-the-art methods.[24, 25] ANR is computationally very fast as opposed to most other SR methods[23] which is a very desirable feature in our setting. ANR creates training data from $\boldsymbol{y}_i$ and $\boldsymbol{y}$, by calculating the first and the second gradient images of $\boldsymbol{y}_i$ in all three directions using the Sobel and Laplacian filters. At voxel location j a 3D patch is extracted from each of these gradient images and concatenated to form a feature vector $\boldsymbol{f}_j(\boldsymbol{y}_i)$. ANR uses PCA to reduce the dimensionality of the feature to the order of $\sim 10^2$. SSRv1 (and SSRv2) do not extract continuous voxels as the LR acquisition means neighboring voxels are highly correlated. Our patch dimensions are linearly proportional to the amount of relative blurring in the x, y, and z directions in $\boldsymbol{y}$. This means that patches are cuboids in shape and are longer in the dimension where the blurring is higher. We then calculate the difference image $\boldsymbol{y}_i^d = \boldsymbol{y} - \boldsymbol{y}_i$ and the extracted patch $\boldsymbol{g}_j(\boldsymbol{y}_i^d)$ and pair it with $\boldsymbol{f}_j(\boldsymbol{y}_i)$ to create the training data. Next, ANR jointly learns paired high resolution and low resolution dictionaries, using the K-SVD algorithm. The atoms of the learned dictionary are regarded as cluster centers with each feature vector $\boldsymbol{f}_j(\boldsymbol{y}_i)$ being assigned to one based on the correlation between feature vectors and centers. Cluster centers and their associated feature vectors are used to estimate a projection matrix P_k for every cluster k, by solving a least squares problem such that, $P_k \boldsymbol{f}_j(\boldsymbol{y}_i) = \boldsymbol{g}_j(\boldsymbol{y}_i^d)$. Given an input test image, $\widetilde{\boldsymbol{y_i}}$, feature vectors $\boldsymbol{f}_j(\widetilde{\boldsymbol{y_i}})$ are computed and a cluster center is assigned based on the arg max of the correlation, then the stored P_k is applied to estimate the patch at voxel j in the newly created image $\hat{\boldsymbol{y}}_i$. Overlapping patches are predicted

Algorithm 1 SSRv1 (Complete details can be found in Jog et al.[13])

Data: LR image $\boldsymbol{y}$
Upsample $\boldsymbol{y}$ to isotropic digital resolution
Based on the spatial resolution of $\boldsymbol{y}$, calculate $\boldsymbol{h}$, the slice selection filter
for i=1:n **do**
    Construct a rotation matrix M_i and apply to $\boldsymbol{y}$ to form the rotated image $M_i(\boldsymbol{y})$
    Apply M_i to $\boldsymbol{h}$ to form the rotated filter $M_i(\boldsymbol{h})$
    Generate $\boldsymbol{y}_i = M_i(\boldsymbol{h}) * \boldsymbol{y}$
    Generate $\widetilde{\boldsymbol{y}}_i = \boldsymbol{h} * M_i(\boldsymbol{y})$
    Use ANR to synthesize $\hat{\boldsymbol{y}}_i = \mathrm{ANR}(\boldsymbol{y}_i, \boldsymbol{y}, \widetilde{\boldsymbol{y}}_i)$
end for
Apply FBA to get, $\hat{\boldsymbol{x}}_p = \mathrm{FBA}(\boldsymbol{y}, M_1^{-1}(\hat{\boldsymbol{y}}_1), \ldots, M_n^{-1}(\hat{\boldsymbol{y}}_n), p)$

---

and the overlapping voxels have their intensities averaged to produce the final output $\hat{\boldsymbol{y}}_i$. This modified ANR is carried out to estimate each $\hat{\boldsymbol{y}}_i$ where the rotation matrices can be chosen intelligently to cover the Fourier space. ANR on its own can only add information in a single direction of the Fourier domain. However, when run in multiple directions, we are able to add coefficients for more frequencies in the Fourier space. SSRv1 is summarized in Algorithm 1. The flow chart in Fig. 1 shows (Steps 1 & 2) how to construct the training data from the input image, $\boldsymbol{y}$; (Steps 3 & 4) how to generate the rotated images, $\widetilde{\boldsymbol{y_i}}$; (Step 5) how to synthesize the images, $\hat{\boldsymbol{y_i}}$, that have different Fourier extents; and (Step 6) how to undo the rotations so the images can be combined using the Fourier Burst Accumulation to generate the SR image $\hat{\boldsymbol{x}}_p = \mathrm{FBA}(\boldsymbol{y}, M_1^{-1}(\hat{\boldsymbol{y}}_1), \ldots, M_n^{-1}(\hat{\boldsymbol{y}}_n), p)$.

SSRv2 Our first modification to SSRv1 regards the value of p used in the FBA reconstruction. We experimentally observed that peak signal to noise ratio (PSNR) increases as p increases, see Fig. 2(a). However, SSRv1 fixed $p = 2$, which is clearly suboptimal and we therefore consider $p = \infty$. In practical terms, we modify Eqn. 1 to take the maximum $\boldsymbol{Y}_i(\omega)$ over i for each frequency ω. The second modification to SSRv1, was based on the observation that the method is sensitive to the fidelity of the input images to FBA; therefore the interpolation of the rotated images, $\boldsymbol{y}_i$, is of critical importance. We further observed that the original implementation of SSRv1 used builtin rotation functions in Matlab that unneccessarily degraded the rotated images. As an alternative to rotated images through interpolation, we propose when considering rotations that align cardinal axes to compute the rotations via simple reorderings of the interpolated isotropic version of $\boldsymbol{y}$ thus avoiding any interpolations due to rotation—for cardinal axis rotations. Our third change to SSRv1, was initially designed to accelerate the computation. We pad the images to have a digital resolution of the next highest power of 2, the point being to take advantage of a FFT for computation purposes. However, we observed that using a padded image with a FFT had a marginal improvement on the PSNR of the output image, $\hat{\boldsymbol{x}}_\infty$. This may in part be because of interpolation that occurs within the default Matlab Fourier Transform, however the exact nature of this issue remains an open question. The final improvement to SSRv1, involves the space with which the FBA computation was performed. SSRv1 had originally had uncropped the Fourier domain images, however this leads to interpolation issues when doing the $\mathcal{F}^{-1}$. As SSRv2 now keeps images in a power of 2 padded space and uses FFT, the FBA analysis can be done in a power of 2 padded space and inverted efficiently without any unneccessary interpolations. See Fig. 2 for inputs, and outputs of SSRv1 and SSRv2.

4. EXPERIMENTS

We compare SSRv1 and SSRv2 on T_1-weighted Magnetization Prepared Rapid Gradient Echo (MPRAGE) images from 18 subjects of the Neuromorphometrics dataset. The resolution of images in this dataset is 1 mm^3 isotropic and we consider this our HR dataset. We create LR images by modeling a slice selection filter ($\boldsymbol{h}$) based on a slice selection pulse modeled as a truncated sinc function. The slice selection filter itself looks like a jagged rect function. We create LR datasets with slice thicknesses of 2 mm. The in-plane resolution remains 1×1 mm^2.

From the LR data, we generated SR data using both SSRv1 and SSRv2 noting that SSRv1 has been previously shown to be better than state-of-the-art SR methods. Evaluation was done using PSNR by direct comparison between the SR images and the HR images for the 18 subjects with results comparing SSRv1 and SSRv2 are
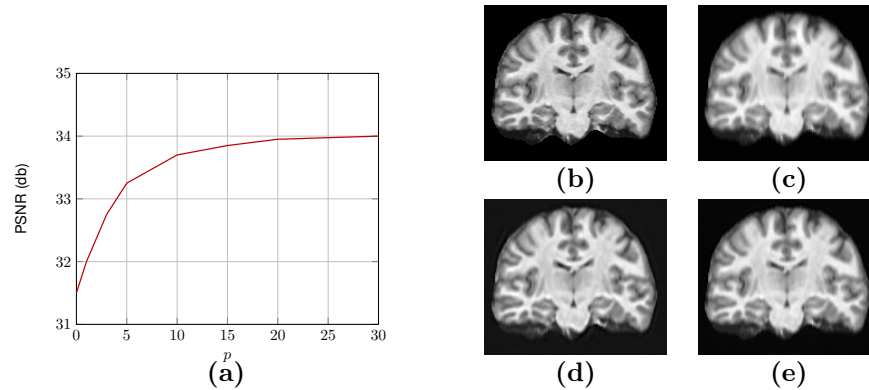
Figure 2. Shown is **(a)** a plot varing p vs. PSNR of $\hat{\boldsymbol{x}}_p$, **(b)** $\boldsymbol{x}$, **(c)** $\boldsymbol{y}$, **(d)** $\hat{\boldsymbol{x}}_\infty$ for SSRv1, and **(e)** $\hat{\boldsymbol{x}}_\infty$ for SSRv2.

Table 1. Mean, standard deviation (Std. Dev.), minimum (Min), and maximum (Max) of the peak signal to noise ratio (PSNR); computed between the HR image, $\boldsymbol{x}$, and the SR image, $\hat{\boldsymbol{x}}_\infty$, generated by both SSRv1 and SSRv2.

Method	PSNR (db)			
	Min	Mean	Std. Dev.	Max
SSRv1	34.27	37.14	1.467	39.10
SSRv2	34.34	37.56	1.430	39.50

shown in Table 1. To avoid an unfair comparison between SSRv1 and SSRv2, we set $p = \infty$ in SSRv1 had we not done this SSRv2 would be dramatically better than SSRv1. A paired Wilcoxon Rank Sum test comparing SSRv1 and SSRv2 with respect to the PSNR values has a p-value of 1.526×10^{-5} demonstrating significant improvement.

5. DISCUSSION AND CONCLUSION

We have described SSRv2 an improvement on SSRv1 for MRI super-resolution that uses the existing high frequency information in the given LR image to estimate the SR image.

Acknowledgments

REFERENCES

[1] Hardie, R. C., Barnard, K. J., Bognar, J. G., and Armstrong, E. E., "Joint MAP registration and high-resolution image estimation using a sequence of undersampled images," *IEEE Trans. Imag. Proc.* **6**(2), 1621–1633 (1997).

[2] Greenspan, H., Oz, G., Kiryati, N., and Peled, S., "MRI inter-slice reconstruction using super-resolution," *Mag. Reson. Med.* **20**(5), 437–446 (2002).

[3] Peeters, R. R., Kornprobst, P., Nikolova, M., Sunaert, S., Vieville, T., Malandain, G., Deriche, R., Faugeras, O., Ng, M., and Van Hecke, P., "The use of super-resolution techniques to reduce slice thickness in functional MRI," *Int. J. Imaging Syst. Technol.* **14**(3), 131–138 (2004).

[4] Bai, Y., Han, X., and Prince, J. L., "Super-resolution Reconstruction of MR Brain Images," in [*Proceedings of the Conference on Information Sciences and Systems (CISS 2004)*], 1358–1363 (2004).

[5] Roy, S., Carass, A., and Prince, J. L., "Synthesizing MR contrast and resolution through a patch matching technique," in [*Proceedings of SPIE Medical Imaging (SPIE-MI 2010), San Diego, CA, February 14-17, 2010*], **7623**, 7623 – 7623 – 9 (2010).

[6] Rousseau, F., "A non-local approach for image super-resolution using intermodality priors," *Medical Image Analysis* **14**(4), 594–605 (2010).

[7] Manjón, J. V., Coupé, P., Buades, A., Fonov, V., Collins, D. L., and Robles, M., "Non-local MRI upsampling," *Medical Image Analysis* **14**(6), 784–792 (2010).

[8] Manjón, J. V., Coupé, P., Buades, A., , Collins, D. L., and Robles, M., "MRI superresolution using self-similarity and image priors," *International Journal of Biomedical Imaging* **425891**, 11 (2010).

[9] Roohi, S., Zamani, J., Noorhosseini, M., and Rahmati, M., "Super-resolution MRI images using Compressive Sensing," in [*Electrical Engineering (ICEE), 2012 20th Iranian Conference on*], 1618–1622 (2012).

[10] Plenge, E., Poot, D. H. J., Bernsen, M., Kotek, G., Houston, G., Wielopolski, P., van der Weerd, L., Niessen, W. J., and Meijering, E., "Super-Resolution Reconstruction in MRI: Better Images Faster?," in [*Proceedings of SPIE Medical Imaging (SPIE-MI 2012), San Diego, CA, February 4-9, 2012*], **8314**, 83143V–83143V–8 (2012).

[11] Rousseau, F. and Studholme, C., "A supervised patch-based image reconstruction technique: Application to brain MRI super-resolution," in [*10ᵗʰ International Symposium on Biomedical Imaging (ISBI 2013)*], 346–349 (2013).

[12] Jog, A., Carass, A., and Prince, J. L., "Improving magnetic resonance resolution with supervised learning," in [*11ᵗʰ International Symposium on Biomedical Imaging (ISBI 2014)*], 987–990 (2014).

[13] Jog, A., Carass, A., and Prince, J. L., "Self super-resolution for magnetic resonance images," in [*19ᵗʰ International Conference on Medical Image Computing and Computer Assisted Intervention (MICCAI 2016)*], *Lecture Notes in Computer Science* **9902**, 553–560, Springer Berlin Heidelberg (2016).

[14] Mahapatra, D., Bozorgtabar, B., Hewavitharanage, S., and Garnavi, R., "Image Super Resolution Using Generative Adversarial Networks and Local Saliency Maps for Retinal Image Analysis," in [*20ᵗʰ International Conference on Medical Image Computing and Computer Assisted Intervention (MICCAI 2017)*], *Lecture Notes in Computer Science*, 382–390, Springer Berlin Heidelberg (2017).

[15] Zhao, C., Carass, A., Dewey, B. E., and Prince, J. L., "Self super-resolution for magnetic resonance images using Deep Networks," in [*15ᵗʰ International Symposium on Biomedical Imaging (ISBI 2018)*], (2018).

[16] Greenspan, H., "Super-Resolution in Medical Imaging," *The Computer Journal* **52**(1), 43–63 (2008).

[17] Park, S. C., Park, M. K., and Kang, M. G., "Super-resolution image reconstruction: a technical overview," *IEEE Signal Processing Magazine* **20**(3), 21–36 (2003).

[18] Jog, A., Carass, A., Roy, S., Pham, D. L., and Prince, J. L., "MR Image Synthesis by Contrast Learning On Neighborhood Ensembles," *Medical Image Analysis* **24**(1), 63–76 (2015).

[19] Huang, J.-B., Singh, A., and Ahuja, N., "Single Image Super-Resolution from Transformed Self-Exemplars," in [*2015 IEEE Conference on Computer Vision and Pattern Recognition (CVPR)*], 5197–5206 (2015).

[20] Rueda, A., Malpica, N., and Romero, E., "Single-image super-resolution of brain MR images using overcomplete dictionaries," *Medical Image Analysis* **17**(1), 113–132 (2013).

[21] Delbracio, M. and Sapiro, G., "Burst Deblurring: Removing Camera Shake Through Fourier Burst Accumulation," in [*2015 IEEE Conference on Computer Vision and Pattern Recognition (CVPR)*], 2385–2393 (2015).

[22] Delbracio, M. and Sapiro, G., "Removing Camera Shake via Weighted Fourier Burst Accumulation," *IEEE Trans. Imag. Proc.* **24**(11), 3293–3307 (2015).

[23] Timofte, R., De, V., and Van Gool, L., "Anchored Neighborhood Regression for Fast Example-Based Super-Resolution," in [*2013 IEEE International Conference on Computer Vision (ICCV)*], 1920–1927 (2013).

[24] Yang, J., Wright, J., Huang, T. S., and Ma, Y., "Image Super-resolution via Sparse Representation," *IEEE Trans. Imag. Proc.* **19**(11), 2861–2873 (2010).

[25] Freeman, W. T., Jones, T. R., and Pasztor, E. C., "Example-based super-resolution," *IEEE Computer Graphics and Applications* **22**(2), 56–65 (2002).